Progress In Electromagnetics Research B, Vol. 88, 35–52, 2020

Predicting Performance Characteristics of Double Elliptical Micro-Strip Patch Antenna for Radiolocation Applications Using Response Surface Methodology

Jerry V. Jose[1, *], Aruldas S. Rekh[1], and Manayanickal J. Jose[2]

Abstract—Double Elliptical Micro-strip Patch Antenna (DEMPA) is a newer family of patch antennas which possesses higher design flexibility and has greater potential for getting miniaturized than Elliptical Micro-strip Patch Antenna (EMPA). The DEMPA is made out of a Double Elliptical Patch (DEP) which is designed as a combination of two half-elliptical patches either with a common minor axis and two different semi-major axes or with a common major axis and two different semi-minor axes. There are only two design parameters for an EMPA, its semi-major axis and semi-minor axis, whereas a DEMPA has three because of either two different semi-major axes or two different semi-minor axes. A parametric study is required to understand the relationship among these three design parameters and antenna characteristics such as return loss, impedance, resonant frequency, and gain. The present work is a statistical study, using the concept of Design of Experiments (DOE), of the impact of these design parameters on the return loss at resonant frequency within the frequency band of 8.50 GHz–10.55 GHz which has been earmarked for radiolocation applications by regulating agency. The Central Composite Design (CCD) technique in the Response Surface Methodology (RSM) of DOE has been employed here to develop empirical relationship between the design parameters and response variable. Numerical models were developed using Ansoft's HFSS as per the design matrix provided by Minitab. The concept of DOE helped to establish statistically significant parametric relationship between the design parameters and antenna return loss with the minimum amount of design effort. The predictive ability of regression model was confirmed by using numerical models of two DEMPAs that were not utilized to build the empirical relationship, one among which had been fabricated, tested and reported in literature.

1. INTRODUCTION

The Micro-Strip Patch Antenna (MSPA) has applications in several fields of wireless communication such as satellite communication, mobile communication, telemedicine, radiolocation, Worldwide Interoperability for Microwave Access (WiMax) based communication, biomedical radiators, radio altimeters, mobile radio, and direct broadcast services. Antenna arrays in which patches are arranged as constitutive elements are used for Wi-Fi applications [1, 2]. In fact, MSPA is the most widely used type of printed-circuit antenna, and the other types are stripline slots and printed-circuit board dipoles and monopoles [3]. Printing dipoles or monopoles in a dielectric substrate and feeding by a micro-strip line [4] is a means for low-cost fabrication. Coming back to MSPAs, any effort in the direction of antenna miniaturization will further improve the range of its applications. In general, there are two broad ways to miniaturize MSPAs. One way is to change the material properties of its substrate so as to reduce the effective wavelength in the substrate region, and the second way is to change its shape so as to increase

Received 15 May 2020, Accepted 18 August 2020, Scheduled 26 August 2020
* Corresponding author: Jerry V. Jose (jerryv@karunya.edu.in).
[1] Karunya Institute of Technology and Sciences, Coimbatore, Tamil Nadu, India. [2] Govt. College of Engineering Kannur, Kerala, India.

the electrical size [5]. The way of bringing about changes in the shape of MSPAs have been successfully tried by several researchers to miniaturize it, and these were mostly manipulations with additions to or deletions from regular basic shapes such as rectangle, circle, triangle, and ellipse. A significant amount of literature focused on fractal shapes too. MSPAs of several variants of the aforesaid basic shapes were reported in literature. As long as the design flexibility of these basic shapes remains unchanged, the scope of further miniaturization is limited. Design flexibility of MSPA in turn depends on the number of degrees of freedom in design with respect to the shape. The more the number of degrees of freedom is, the higher the design flexibility will be. It was in this backdrop, the authors suggested a new family of MSPAs called 'Double Elliptical Micro-strip Patch Antenna (DEMPA)' where a Double Elliptical Patch (DEP) had one additional degree of freedom in the design compared to an Elliptical Micro-strip Patch Antenna (EMPA) [2, 3]. For a DEMPA with equal horizontal semi-major axes and unequal vertical semi-minor axes, the radiation properties were found similar to the corresponding EMPA even when the effective patch area was reduced by 10.714% [7]. For DEMPA with unequal horizontal semi-major axes and equal vertical semi-minor axes, the antenna characteristics were similar to the corresponding EMPA even when the effective patch area was reduced by 8.33% [6]. Antenna miniaturization in this order was achieved because of the increased design flexibility due to an additional degree of freedom in design.

Further research in the effectiveness of double elliptical shape in antenna miniaturization necessitates a detailed parametric study which will establish an empirical relationship between the shape-related design parameters and response variables such as return loss and/or resonant frequency. The geometric design parameters may have direct effects as well as interaction effects on the response variables. Both these effects need to be taken into consideration in order to assess the radiation behavior of DEMPA while going for miniaturization. The concept of Design of Experiments (DOE), particularly its Response Surface Methodology (RSM), is well suited for such a study even though the use of this technique was reported very little in the literature of electromagnetic research. A cavity backed, folded-slot antenna was characterized using DOE technique to study the effects of antenna dimensions on resonant frequency and reflection coefficient at resonance [8]. A full factorial design with no replication was employed here to obtain regression equations for the aforesaid response variables. An empirical model for the return loss of flip-chip CPW interconnect was developed with the help of simulation runs conducted as per the design matrix provided by DOE [9]. The DOE reportedly enabled trimming the design space to a manageable size, formulating the empirical relations using only statistically significant terms and incorporating the interaction effects between parameters. Geometric parameters of the symmetric toggle RF MEMS switch were optimized using RSM to minimize the switch pull-in voltage [10]. The most significant factors affecting the pull-in voltage, which was the response, were screened out using Plackett-Burman screening design and analysis of variance (ANOVA) in DOE. Optimization of these significant parameters was performed using Box-Behnken design based RSM. Regression models for responses such as return loss and resonant frequency were developed, and a multi-response optimization was conducted for reconfigurable Sierpinski fractal antenna with the help of RSM in DOE [11]. The response values were created through simulations. The interaction effects of three design parameters on return loss and resonant frequency were also studied. The technique of full factorial design in DOE becomes costly, especially when the number of design parameters increases beyond three. The required number of experimental runs increases exponentially with the increase in number of design parameters. Orthogonal fractional experiments were demonstrated to be highly efficient compared to the full factorial design for antenna optimization in terms of the number of experimental runs [12]. Electromagnetic Band Gap (EBG) structures for MSPAs were modeled and optimized using RSM [13]. The geometrical parameters of EBG structure were the design parameters, and upper and lower band gap frequencies were the response parameters. The response values were collected through Electromagnetic (EM) simulations using an FEM based solver, Ansoft HFSS.

The reported use of RSM in electromagnetic research is less whereas in the areas such as chemical engineering and manufacturing engineering, RSM has become an established practice to formulate empirical relationships between the required set of design parameters and response variables [14–17]. The present paper is an attempt to employ the concept of RSM to study the parametric relationship between the design parameters of DEMPA and Return Loss (RL) at resonant frequency. The length of vertically aligned minor axis (d), the length of semi-major axis of left half-ellipse (a_1), and the length

of semi-major axis of right half-ellipse (a_2) of the DEMPA were the design parameters. The DEMPA has been developed from an elliptical shape referral antenna [18] with lengths of semi-major axis and semi-minor axis being 9.0 mm and 7.0 mm, respectively. An extensive pilot study on parametrical relationship was conducted on this DEMPA using the method of varying one-factor-at-a-time which revealed that when a_1, a_2, and d were varied within the ranges of 4.0 mm–9.0 mm, 4.0 mm–9.0 mm, and 10.0 mm–14.0 mm, respectively, all the DEMPAs had one of their resonant frequencies fallen within a narrow band of 8.52 GHz–10.43 GHz having a width of just 1.91 GHz. All these DEMPAs were of substantially different patch areas, and all of them could produce resonance within this narrow band. In other words, all these DEMPAs had similar radiation performances within this narrow band. The minimum and maximum patch areas were 62.8 mm^2 and 197.82 mm^2, respectively, and percentage of patch area reduction between them was 68.25%. It is shown that even for the DEMPA with 68.25% less patch area, the resonant frequency falls within this narrow band. As per the regulatory agency of International Telecommunication Union (ITU), the frequency band of 8.50 GHz–10.55 GHz is set aside for radiolocation applications, and the band of 8.52 GHz–10.43 GHz falls well within this. Hence, there are a lot of possibilities for miniaturizing antennas for radiolocation applications using the DEPs under consideration. This is the motivation behind conducting an RSM based parametric study on DEMPAs developed from the referral antenna with respect to the frequency band of 8.50 GHz–10.55 GHz which has been allotted to radiolocation applications.

The solution frequency for simulations in HFSS has been conveniently chosen as 9.85 GHz. The RL is obtained at a resonant frequency within the band of 8.50 GHz–10.55 GHz and close to the solution frequency of 9.85 GHz. Ansoft HFSS, the FEM based EM solver, was used to develop numerical models by simulation in which the response values were collected. Section 2 provides construction details of DEMPA. Section 3 explains the technique of RSM, and the subsequent sections describe the development of model, results, and discussions. Main effects and interaction effects of design parameters on RL were discussed. Predictive ability of the regression model obtained was confirmed with the help of two numerically modeled DEMPAs, and one among them had been fabricated whose details were reported in the authors' previous paper [6]. The simulated radiation characteristics of radiation pattern, peak gain curve, radiation efficiency curve, axial ratio curve, and distribution of surface currents of previously fabricated DEMPA were provided and discussed. The RL value for fabricated antenna was found close to its values from numerical and regression models.

2. DOUBLE ELLIPTICAL MICRO STRIP PATCH ANTENNA

A DEMPA is made out of a DEP which is developed from a double ellipse. The double ellipse is a combination of two half-ellipses having either the common minor axis and different semi-major axes or the common major axis and different semi-minor axes [6]. A DEP is characterized in terms of its axis of symmetry and its orientation. There are two axes of symmetry for an elliptical patch but only one for a DEP. The symmetry of DEP may be arranged along horizontal, vertical axis, or inclined at an angle to the horizontal axis. For a DEP with the same vertical minor axis and different horizontal semi-major axes, the axis of symmetry lies in the direction of major axis. The axis of symmetry lies in the direction of minor axis when the DEP has the same horizontal major axis and different vertical semi-minor axes. The DEP with axis of symmetry along the direction of horizontal semi-major axes may be designated as $\mathrm{DEP_{mah}}$, and the DEP with axis of symmetry along the direction of vertical semi-minor axes may be designated as $\mathrm{DEP_{miv}}$ [7]. The corresponding antennas are denoted by $\mathrm{DEMPA_{mah}}$ and $\mathrm{DEMPA_{miv}}$. Fig. 1 shows the schematic representation of $\mathrm{DEP_{mah}}$ and $\mathrm{DEP_{miv}}$.

In the present work, an EMPA designed for the UWB applications [18] was used as the referral antenna for developing $\mathrm{DEMPA_{mah}}$. The lengths of semi-major axis and semi-minor axis of this EMPA were 9.0 mm and 7.0 mm, respectively, and the elliptical patch was arranged in the antenna with its major axis lying horizontally.

3. RESPONSE SURFACE METHODOLOGY (RSM)

The RSM is a collection of mathematical and statistical techniques useful for the modeling and analysis of problems in which a response of interest is influenced by several variables, and the objective is to

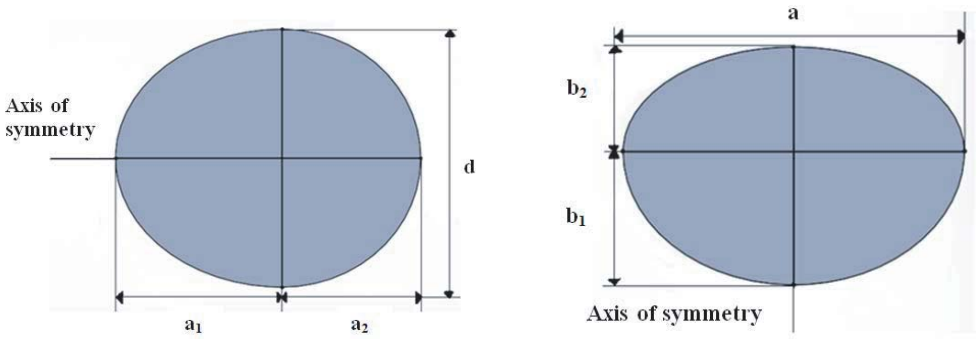

(a) (b)

Figure 1. Schematic representation of (a) DEP_{mah} and (b) DEP_{miv} [7].

optimize this response [19]. This method helps to model and optimize a response by conducting the minimum number of experimental runs. The unknown relationship between the independent variables (input variables) and the output variables (responses) is approximated with the help of either first-order models or second-order models or both. If a linear function of input variables can model the response variable well, then the approximating function will be a first-order model as in Eq. (1), and if there is a curvature in the system, usually a second-order model as in Eq. (2) will be used for approximation [19].

$$y = \beta_0 + \beta_1 x_1 + \beta_2 x_2 + \ldots + \beta_k x_k + \epsilon \tag{1}$$

$$y = \beta_0 + \sum_{i=1}^{k} \beta_i x_i + \sum_{i=1}^{k} \beta_{ii} x_i^2 + \sum_{i<j} \sum \beta_{ij} x_i x_j + \epsilon \tag{2}$$

where 'x' represents the independent variable; 'β' values are coefficients; and ϵ is the error or noise observed in the response 'y'. From the regression model thus obtained, the insignificant terms are avoided by conducting repeated ANOVA. Also, the direct effects and interaction effects of independent variables on response variable can be determined and analyzed. The response variable can be optimized, and the optimum values of input variables may be found. The RSM begins with creating a design matrix for conducting the experimental runs. The independent (input) variables, the range of each variable and their levels are required for this. The design matrix may be created as per either Central Composite Design (CCD) or Box-Behnken method. In the present work, design matrix has been developed using CCD. The values of response variable may be collected by conducting either experiments followed by measurements or simulation runs as per the run order in the design matrix. The total number of runs (N) required for CCD is

$$N = 2^n + 2n + n_{cp} \tag{3}$$

where 'n' is the number of input variables, and 'n_{cp}' is the number of replicates at the central points. In the present work, there were three input variables, and hence the total number of experimental runs required was 20.

4. DEVELOPMENT OF REGRESSION MODEL

4.1. Creating Design Matrix Using CCD

Modeling and analysis of the response variable, RL at the resonant frequency, of DEMPA was performed using RSM in the statistical software Minitab. Three design parameters were the length of vertically aligned minor axis (d), the length of semi-major axis of left half-ellipse (a_1), and the length of semi-major axis of right half-ellipse (a_2) of the $\text{DEMPA}_{\text{mah}}$. Table 1 shows the input variables along with their units and symbols and their levels in coded and uncoded forms. The design matrix developed using CCD in RSM in uncoded values is shown in Table 2.

Table 1. Input variables and their levels in coded and uncoded forms in CCD.

Input variable	Symbol	Levels of coded variables				
		$-\alpha$ -1.682	Low -1	Medium 0	High $+1$	$+\alpha$ $+1.682$
Length of minor axis (mm)	d	8.6364	10	12	14	15.3636
Length of semi-major axis of left half-ellipse (mm)	a_1	2.2955	4	6.5	9	10.7045
Length of semi-major axis of right half-ellipse (mm)	a_2	2.2955	4	6.5	9	10.7045

Table 2. The design matrix with response values in RSM.

Standard order	Run order	Input variable in uncoded form			Response
		d (mm)	a_1 (mm)	a_2 (mm)	Return Loss (RL) in dB
6	1	14.0000	9.0000	4.0000	−26.2593
8	2	14.0000	9.0000	9.0000	−40.1495
19	3	12.0000	6.5000	6.5000	−41.1435
17	4	12.0000	6.5000	6.5000	−41.1435
14	5	15.3636	6.5000	6.5000	−26.2774
15	6	12.0000	6.5000	6.5000	−41.1435
18	7	12.0000	6.5000	6.5000	−41.1435
12	8	12.0000	6.5000	10.7045	−39.73
1	9	10.0000	4.0000	4.0000	−16.0715
7	10	14.0000	4.0000	9.0000	−21.923
4	11	10.0000	9.0000	9.0000	−39.4218
2	12	10.0000	9.0000	4.0000	−28.6236
20	13	12.0000	6.5000	6.5000	−41.1435
9	14	12.0000	2.2955	6.5000	−15.5407
16	15	12.0000	6.5000	6.5000	−41.1435
3	16	10.0000	4.0000	9.0000	−27.045
5	17	14.0000	4.0000	4.0000	−18.7699
10	18	12.0000	10.7045	6.5000	−40.8318
11	19	12.0000	6.5000	2.2955	−16.1361
13	20	8.6364	6.5000	6.5000	−26.8522

4.2. Modeling and Simulation of DEMPAs Using HFSS and Recording Responses

The High Frequency Structure Simulator (HFSS), a Finite Element Method (FEM) based solver for electromagnetic structures from Ansoft, was used to design the $\text{DEMPA}_{\text{mah}}$. For each run in the design matrix from Minitab, corresponding values of input parameters were used to design the antenna, and full wave electromagnetic simulations were carried out. The simulated values of the response variable (return loss) were recorded in Minitab. The simulations were conducted at a solution frequency of 9.85 GHz, and the RL is the return loss at the resonant frequency within the band of 8.50 GHz–10.55 GHz and close to

Table 3. The resonant frequency corresponding to each value of RL in the design matrix.

Run order	Return Loss (RL) in dB	Resonant frequency in GHz
1	−26.2593	9.835
2	−40.1495	9.947
3	−41.1435	9.96
4	−41.1435	9.96
5	−26.2774	9.975
6	−41.1435	9.96
7	−41.1435	9.96
8	−39.73	9.891
9	−16.0715	9.614
10	−21.923	9.877
11	−39.4218	8.52
12	−28.6236	9.953
13	−41.1435	9.96
14	−15.5407	9.667
15	−41.1435	9.96
16	−27.045	9.94
17	−18.7699	10.43
18	−40.8318	9.8
19	−16.1361	9.831
20	−26.8522	10.11

the solution frequency. The resonant frequency corresponding to each value of RL in the design matrix is given in Table 3. The substrate material used for the design of antenna was FR-4, with a relative dielectric constant $\varepsilon_r = 4.4$ and thickness $h = 1$ mm. The length (L) and width (W) of FR-4 substrate were 40.0 mm and 38.0 mm, respectively. The width of micro-strip feed line was 1.6 mm, and the length of feed was 20.7 mm. The dimensions of ground plane were 38.0 mm and 20.0 mm, respectively. The double-elliptical patch and the ground plane were modeled with the same metallic material.

4.3. Analysis of Response Surface Design

The empirical model after repeated ANOVA for the response variable RL is given by,

$$\begin{aligned} RL \;=\; & 231.747 - a_1 \times 12.0184 - a_2 \times 11.7745 - d \times 30.0514 + (a_1)^2 \\ & \times 0.714555 + (a_2)^2 \times 0.728878 + d^2 \times 1.25981 \end{aligned} \tag{4}$$

The ANOVA Table for the RL before conducting the repeated ANOVA is given in Table 4. The final regression model was formulated after removing the insignificant terms identified with the help of their p values (Probability value) with 95% confidence level, and this model was found to be quadratic in nature.

5. RESULTS AND DISCUSSIONS

The statistically significant regression model for RL was found to be a quadratic equation. The terms in Table 4 for which the p values were < 0.05 were ascertained to be significant and other terms insignificant. For these significant terms, the F values were reasonably high. Table 5 gives the statistical parameters obtained from ANOVA for RL. The R-squared and adjusted R-squared values were obtained as 97.25%

Table 4. ANOVA Table for response surface quadratic model for Return Loss.

Source	Degree of Freedom (DF)	Sequential Sum of Squares (Seq SS)	Adjusted Sums of Squares (Adj SS)	Adjusted Mean Squares (Adj MS)	F	p	Remarks
Regression model	9	1900.99	1900.99	211.221	58.04	0.000	Significant
a_1	1	635.75	635.75	635.751	174.71	0.000	Significant
a_2	1	451.16	451.16	451.163	123.98	0.000	Significant
d	1	1.85	1.85	1.850	0.51	0.492	Significant
a_1^2	1	190.11	287.43	287.432	78.99	0.000	Significant
a_2^2	1	239.34	299.07	299.070	82.19	0.000	Significant
d^2	1	365.96	365.96	365.959	100.57	0.000	Significant
a_1a_2	1	13.94	13.94	13.944	3.83	0.079	Insignificant
a_1d	1	0.08	0.08	0.077	0.02	0.887	Insignificant
a_2d	1	2.79	2.79	2.795	0.77	0.401	Insignificant
Residual error	10	36.39	36.39	3.639			
Lack of fit	5	36.39	36.39	7.278			
Pure error	5	0.00	0.00	0.000			
Total	19	1937.38					

Table 5. Statistical parameters obtained from ANOVA for Return Loss.

No.	Statistical parameters	Value
1	Standard error of the regression (S)	2.02305
2	R-squared (R-Sq)	97.25%
3	Predicted R-squared (R-Sq (pred))	91.57%
4	Adjusted R-squared (R-Sq (adj))	95.99%
5	Prediction Error Sum of Squares (PRESS)	163.391

and 95.99%. The R-squared value, also known as the Coefficient of Determination, is a statistical measure of how close the data are to the fitted regression line. It is defined as the percentage of the response parameter variation that can be explained by the model. The R-squared value varies between 0% and 100%. If the model can explain all the variation of response parameter around its mean, then its R-squared value will be 100%. If the model is unable to explain any of the variation of response parameter around its mean, then its R-squared value will be 0%. The R-squared value of 97.25% demonstrates a good fit of the model to the data. In other words, 97.25% of the variation in RL can be explained by the model. The adjusted R-squared value is a variation of the R-squared statistic that has been adjusted for the number of factors in the model. In other words, it is a statistic that is adjusted for the size of the model [19]. The high adjusted R-squared value as much as 95.99% indicates that only significant terms are added to the model. The predicted R-squared value for the RL is 91.57%, and it indicates that about 91% of the variability in new data could be explained by the model. The PRESS statistic is a measure of how well the model will predict the new data and 163.391, being a low value of PRESS, which shows that the model is a good predictor.

5.1. Analysis of Residual Plots

Fig. 2 provides the Standardized Residual versus Order plot, Standardized Residual versus Fits plot and Normal Probability plot of residuals. The Standardized Residual versus Fits plot is seen as an unstructured plot, and the points are scattered at random. The randomness in this plot ensures that the assumption of constant variance is valid. In other words, for each level of factors, the variance is constant. So, the transformation of response variable was not needed. The standardized residuals lie within the range of $(-3, 3)$, and hence there is no possibility of any outliers. It is observed that the Normal Probability plot of residuals is almost a straight line, and hence the assumption of normality also holds well. The Standardized Residual versus Order plot is an indication of whether the residual terms can be considered independent or not. Here, there are not any visible trends in plot, and the residuals appear randomly on either side of the zero residual line, and hence it may be concluded that the regression assumption is satisfied.

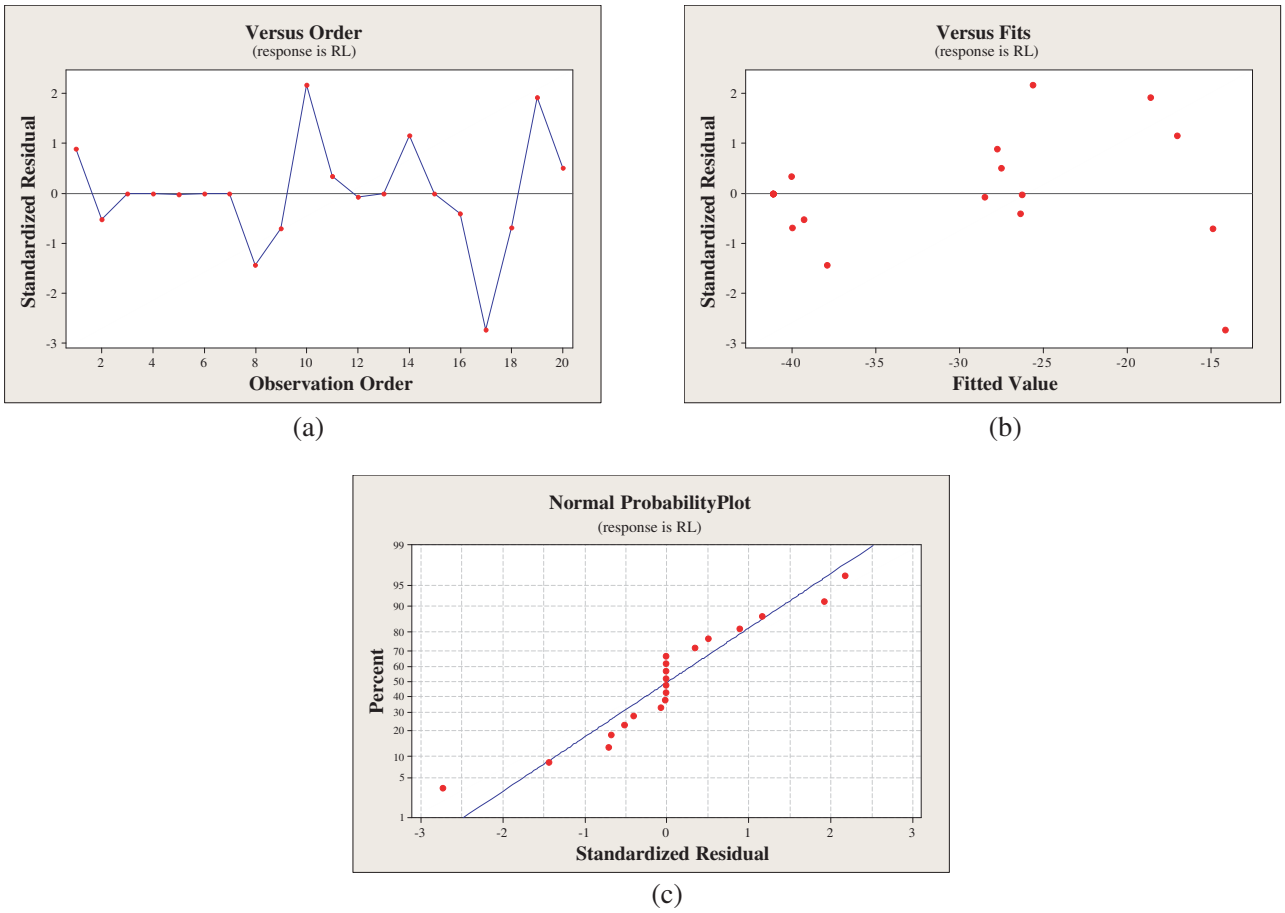

Figure 2. (a) Standardized Residual versus Order plot, (b) Standardized Residual versus Fits plot, (c) Normal Probability plot of residuals.

5.2. Main Effects Plot and Interaction Plot

The Main Effects plot and Interaction plot for the response variable Return Loss (RL) are given in Fig. 3. There will be main effect with respect to a parameter when there are different response values for different levels of that parameter. The Main Effects plot with respect to a parameter shows the average response for different factor levels of that parameter, by combining the effects of other variables on the response as if all the variables are independent. The main effect is said to be positive, if the slope

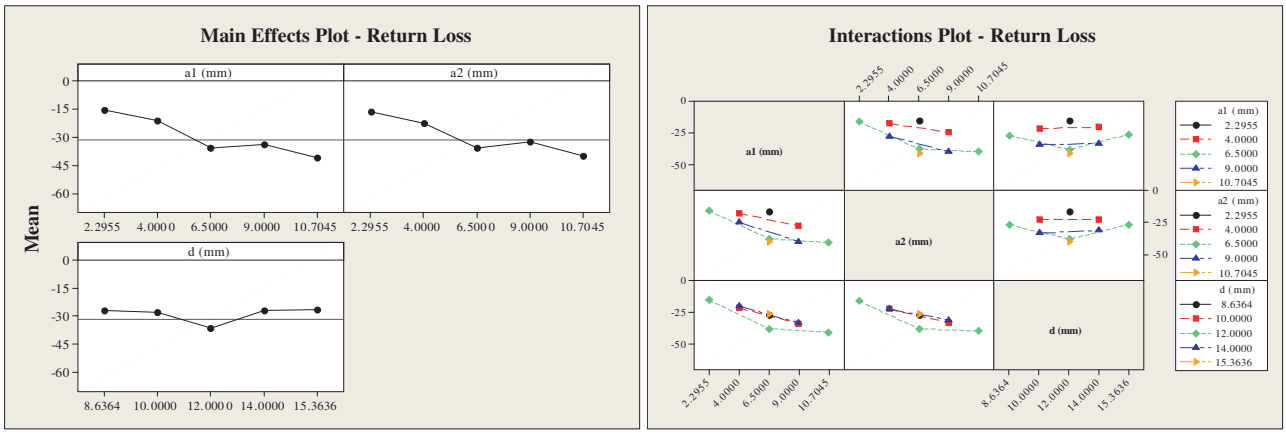

(a) (b)

Figure 3. (a) Main Effects plot for Return Loss, (b) Interactions plot for Return Loss.

of the plot is positive. If the slope is negative, the main effect is said to be negative. The zero slope of the plot indicates that there is no main effect with respect to that parameter. Main Effects plots for RL with respect to the input parameters a_1, a_2, and d are given in Fig. 3(a). It is clear from Fig. 3(a) that the mean RL increases almost steadily with the increase in a_1. A similar trend is also observed with a_2. The mean RL is found to be insensitive to different factor levels of d except the middle of the range selected. Interaction plots describe the effects on response due to input variables which are not independent. In the present study, the interaction effects have already been judged as statistically insignificant using the information from ANOVA as given in Table 4. The Interactions plot is given in Fig. 3(b).

5.3. Analysis of Contour Plots

Fig. 4 shows the contour plots RL versus d and a_1, RL versus d and a_2, and RL versus a_2 and a_1. The higher values of response parameter in such contour plots are denoted by dark regions, and here, since the response parameter assumes negative value, the light colored regions represent higher response values. The lines of constant response are shown in the contour plots along with their values. Each contour represents a certain height of the response surface.

For the 'RL versus d and a_1' plot, a_2 is held at its mean value of 6.5 mm. It is observed that, within the ranges selected, at higher values of a_1 and around mean value of d, the antenna gives higher return loss. In the 'RL versus d and a_2' plot in which a_1 is held at its mean value of 6.5 mm, the RL is high at higher values of a_2 and around mean value of d. It is evident from the curve for 'RL versus a_2 and a_1' that higher values of RL are obtained at higher values of a_1 and a_2 when d is maintained at its mean value. In general, it can be concluded that, for a $\text{DEMPA}_{\text{mah}}$, the more the lengths of its two different semi-major axes are, the higher the RL will be for a given length of minor axis. In other words, the RL of given $\text{DEMPA}_{\text{mah}}$ increases with the increase in its flatness over the horizontal axis.

5.4. Conducting Confirmatory Tests

The developed regression model can be used to find the return loss of $\text{DEMPA}_{\text{mah}}$ within the given range of input variables such as the length of vertically aligned minor axis (d), the length of semi-major axis of left half-ellipse (a_1), and the length of semi-major axis of right half-ellipse (a_2). The return loss predicted by the regression model will be with respect to the resonant frequency within the frequency band of 8.50 GHz–10.55 GHz and close to the solution frequency of 9.85 GHz. This dependence of return loss on these input parameters is characterized by the response surfaces and contour plots. This model represents the relationship between the input parameters and response adequately, as per the statistical parameters obtained after ANOVA. In order to confirm the true representation of the

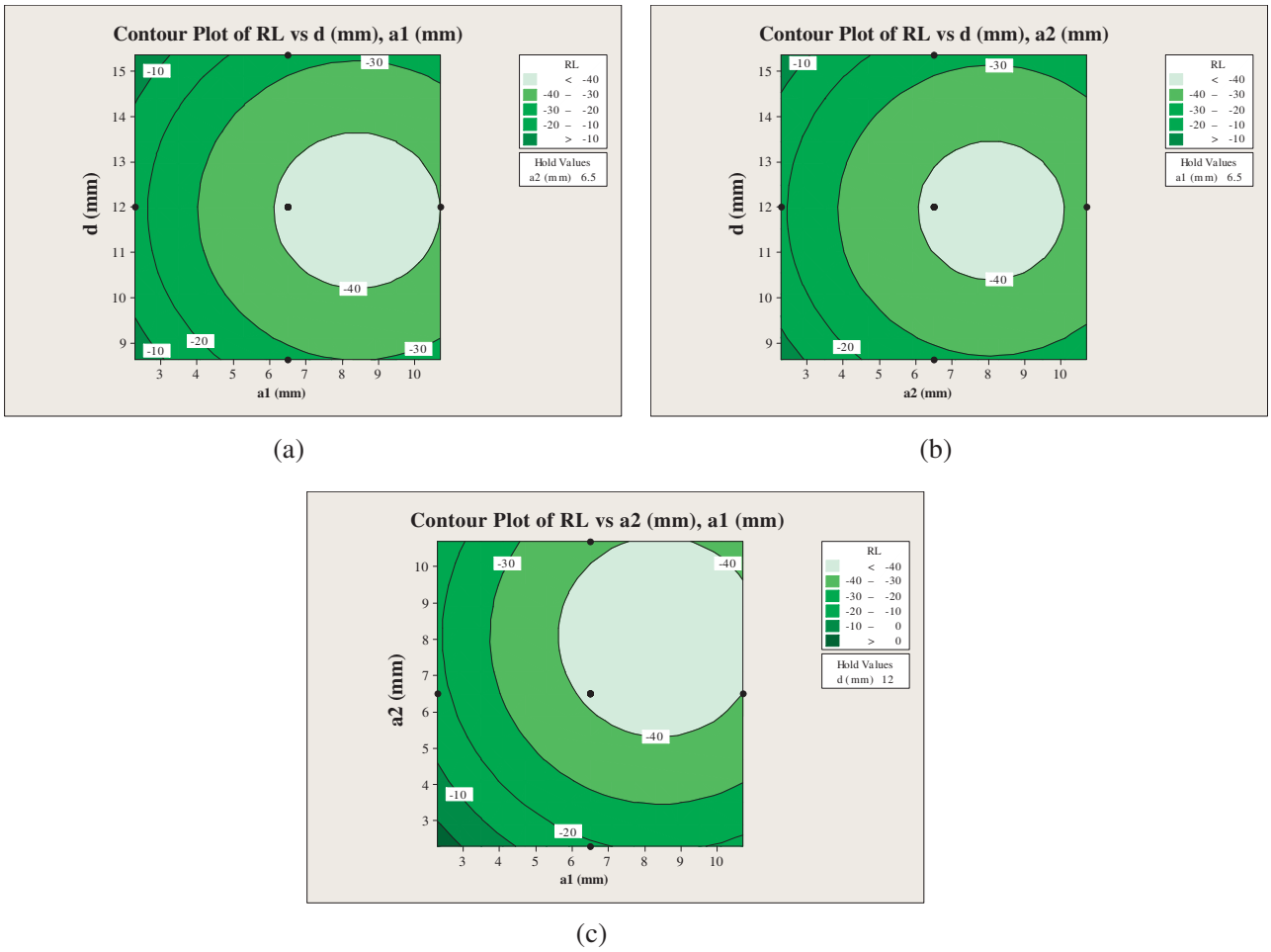

Figure 4. Contour plots of (a) RL versus d and a_1, (b) RL versus d and a_2, (c) RL versus a_2 and a_1.

parametric relationship by the model, two confirmatory tests were conducted. Two DEMPA$_{\text{mah}}$ were modeled in HFSS with values of input parameters which were not included in the earlier design matrix, and their return loss values were determined. These RL values were compared with the responses obtained by using the regression model. The absolute percentage difference in RL values obtained from numerical model and regression model for the first and second confirmatory tests were 7.37% and 6.42%, respectively, which are well within the generally accepted limits. The RL values from numerical model and regression model were very close, thus establishing the true representation of the numerical model by the regression model with reasonable accuracy. Table 6 shows the comparison of RL values from regression model and confirmatory tests using numerical model. The corresponding resonant frequencies for the two DEMPAs obtained from numerical modeling were 10.01 GHz and 10.1922 GHz, respectively.

Table 6. Details of confirmatory experiments.

No.	a_1 (mm)	a_2 (mm)	d (mm)	RL (Regression model) in dB	RL (Numerical model) in dB	% Difference (absolute)
1	9.0	7.5	14.0	−39.6458	−36.9249	7.37
2	5.6	6.5	10.5	−35.5324	−33.3886	6.42

6. FABRICATION AND TESTING OF DEMPA

6.1. Details of Antenna Fabrication and Testing

In order to validate the numerical as well as regression model, details of resonant frequency and RL measurement of a fabricated antenna were required. One of the aforesaid two $\text{DEMPA}_{\text{mah}}$ had been fabricated, tested, and its measurements reported in the authors' earlier paper [6]. The fabricated antenna was of serial number 1 in Table 6. The values of input parameters for the fabricated antenna were $a_1 = 9.0\,\text{mm}$, $a_2 = 7.5\,\text{mm}$, and $d = 14.0\,\text{mm}$, respectively. The solution frequency at which this $\text{DEMPA}_{\text{mah}}$ model was simulated in HFSS was 9.85 GHz. The antenna was fabricated by a chemical etching process called photo-lithographic method in which the unwanted regions of metallic layer as per the designed shape of antenna were removed. An SMA connector with a characteristic impedance of $50\,\Omega$ was used to feed the prototype $\text{DEMPA}_{\text{mah}}$ antenna. The SMA connector was joined to the FR-4 substrate through the process of soldering. At one of the edges of minor axis of double elliptical patch, a micro-strip feed line of width 1.6 mm and length 20.7 mm was placed. The Vector Network Analyzer ENA (E 5071C) was employed to obtain the return loss and VSWR measurements at a lossless laboratory. Fig. 5 shows the top view and bottom view of the fabricated antenna.

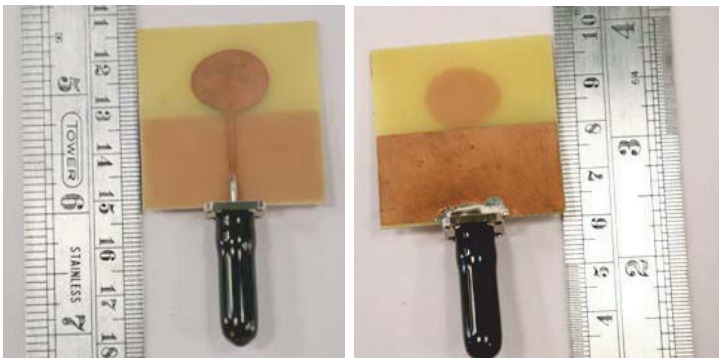

(a) (b)

Figure 5. The fabricated $\text{DEMPA}_{\text{mah}}$ with $a_1 = 9.0\,\text{mm}$, $a_2 = 7.5\,\text{mm}$ and $d = 14.0\,\text{mm}$, (a) top view, (b) bottom view [6].

6.2. Characteristics of DEMPA

6.2.1. Return Loss Curves

For the fabricated antenna, the resonant frequency within the frequency band of 8.50 GHz–10.55 GHz and close to the solution frequency of 9.85 GHz was 9.00 GHz, and the corresponding value of RL was $-33.86\,\text{dB}$ [6]. This is found very close to the RL values from regression model and numerical model as given in Table 6. A comparison of the return loss characteristics of numerically modeled and fabricated antennas within the frequency band of 8.50 GHz–10.55 GHz is shown in Fig. 6(a). It is observed that there is a slight difference in the values of RL and resonant frequency between fabricated and numerically modeled DEMPAs. For RL, this difference is 3.0649 dB (9.05%), and for resonant frequency, it is 1.01 GHz (11.22%). This deviation may be due to the practical aspects and limitations in fabrication and testing which were not considered during modeling and simulations. These may be the level of tolerance considered during the fabrication of DEMPA and soldering of SMA connector, the ground plane effect, and the SMA connector effect. Even though the dielectric loss tangent of FR-4 substrate is a function of frequency, it was kept constant during the simulations. This might have also caused the difference in RL and resonant frequency values between fabricated and simulated antennas. The regression model developed using RSM is thus proved to be capable of accurately predicting the return loss values of DEMPAs within the input parameter range selected (4.0 mm–9.0 mm, 4.0 mm–9.0 mm and

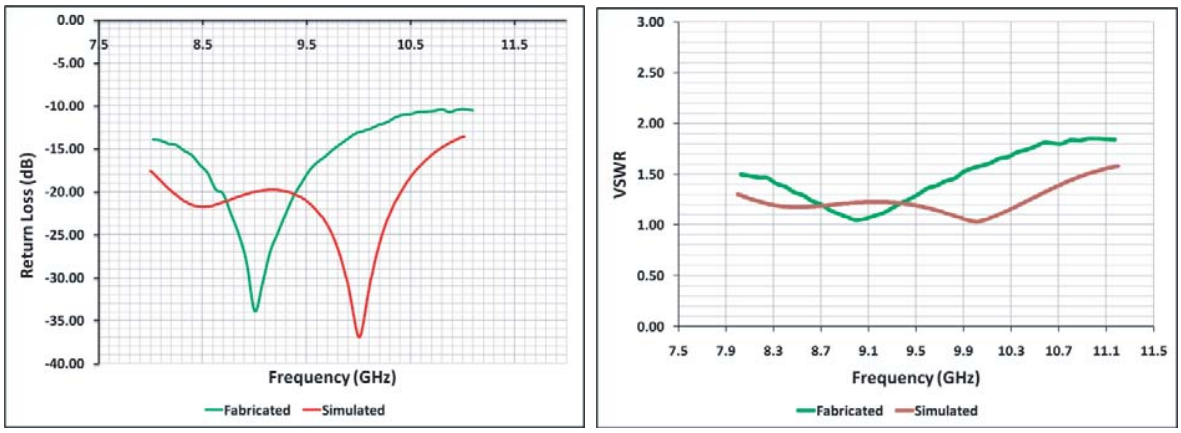

(a) (b)

Figure 6. (a) Return Loss curves, (b) VSWR curves — for fabricated and simulated $\text{DEMPA}_{\text{mah}}$ within the frequency band for radiolocation applications where $a_1 = 9.0\,\text{mm}$, $a_2 = 7.5\,\text{mm}$ and $d = 14.0\,\text{mm}$.

10.0 mm–14.0 mm for a_1, a_2, and d, respectively) and within the frequency band of 8.50 GHz–10.55 GHz, which is earmarked for radiolocation applications.

6.2.2. VSWR Curves

The VSWR curves for fabricated and simulated DEMPAs within this frequency band are shown in Fig. 6(b), and it is clear from the figure that the VSWR values are < 2 throughout the band. The VSWR values at resonance are very close to unity, and in the case of fabricated antenna it indicates a good impedance match between the antenna and feed network.

6.2.3. Peak Gain Curve

The simulated peak gain curve in Fig. 7(a) shows that the $\text{DEMPA}_{\text{mah}}$ with $a_1 = 9.0\,\text{mm}$, $a_2 = 7.5\,\text{mm}$, and $d = 14.0\,\text{mm}$ has fairly good positive gain values within the frequency range for radiolocation applications. The maximum and minimum gain values within this range were found to be 5.06 dB and 3.87 dB at 9.57 GHz and 8.58 GHz, respectively. The observed gain at the resonant frequency of 10.01 GHz was 4.90 dB.

6.2.4. Radiation Efficiency Curve

The simulated Radiation Efficiency curve within the frequency range for radiolocation applications is shown in Fig. 7(b). The $\text{DEMPA}_{\text{mah}}$ with $a_1 = 9.0\,\text{mm}$, $a_2 = 7.5\,\text{mm}$, and $d = 14.0\,\text{mm}$ has the maximum and minimum Radiation Efficiency values of 86.18% and 82.83% at 8.64 GHz and 10.55 GHz, respectively. At the resonant frequency of 10.01 GHz, it has an efficiency of 84.16%. For radiolocation applications, this value of Radiation Efficiency is comparable to that in other research works reported in published literature and is better than [20] where efficiency values were 81.64% and 83.85% at resonant frequencies of 9.18 GHz and 10.8 GHz, respectively.

6.2.5. Radiation Pattern

Simulated far-field radiation patterns of $\text{DEMPA}_{\text{mah}}$ under consideration, captured at the resonant frequency of 10.01 GHz, at E-plane (X-Z) and H-plane (Y-Z) are shown in Fig. 8. The radiation pattern is found nearly omnidirectional at this frequency. The co-polarization and cross-polarization levels are clearly shown. The cross-polarization level in E-plane is found to be acceptable. The cross-polarization level in H-plane is considerably high.

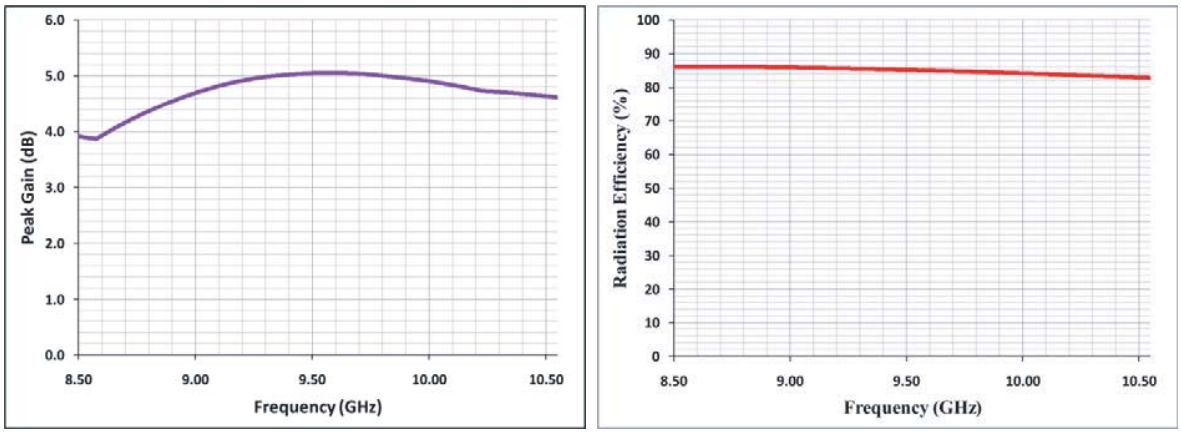

(a) (b)

Figure 7. (a) Simulated Peak Gain curve, (b) Simulated Radiation Efficiency curve — for $\text{DEMPA}_{\text{mah}}$ with $a_1 = 9.0\,\text{mm}$, $a_2 = 7.5\,\text{mm}$ and $d = 14.0\,\text{mm}$ within the frequency range for radiolocation applications.

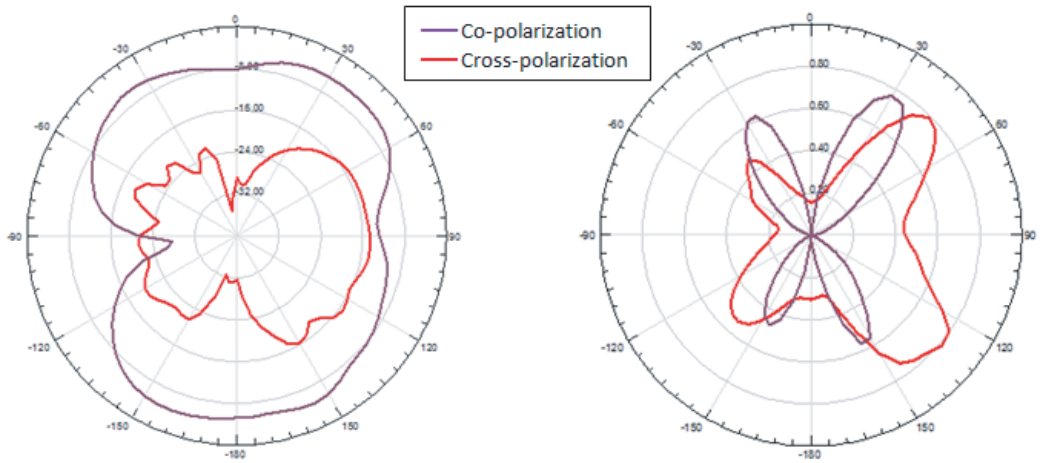

(a) (b)

Figure 8. Simulated far-field radiation patterns of $\text{DEMPA}_{\text{mah}}$ with $a_1 = 9.0\,\text{mm}$, $a_2 = 7.5\,\text{mm}$ and $d = 14.0\,\text{mm}$ at 10.01 GHz, (a) E-plane (X-Z), (b) H-plane (Y-Z).

6.2.6. Axial Ratio Curve

The Axial Ratio curve reveals the type of polarization of antenna. When the axial ratio of an antenna is $\leq 3\,\text{dB}$, it is said to be circularly polarized, and if it is $> 3\,\text{dB}$, it is linearly polarized. Fig. 9(a) shows the variation of axial ratio within the frequency range for radiolocation applications for the $\text{DEMPA}_{\text{mah}}$ with $a_1 = 9.0\,\text{mm}$, $a_2 = 7.5\,\text{mm}$, and $d = 14.0\,\text{mm}$. At the resonant frequency of 10.01 GHz, axial ratio was found to be 39.23 dB. Hence, the $\text{DEMPA}_{\text{mah}}$ under consideration is linearly polarized.

6.2.7. Surface Current Distribution

The distribution of surface current over the patch and ground plane of $\text{DEMPA}_{\text{mah}}$ with $a_1 = 9.0\,\text{mm}$, $a_2 = 7.5\,\text{mm}$, and $d = 14.0\,\text{mm}$ at the resonant frequency of 10.01 GHz is shown in Fig. 9(b). In order to capture the profile of maximum current distribution, the image was taken as looking from the negative Z axis, when the bottom surface of patch was on X-Y plane, and its thickness was along the positive

Table 7. Comparison of effective patch area of the fabricated DEMPA with that of various patch antennas from literature for radiolocation applications.

Reference	Antenna size details (mm)	Antenna design details	Effective patch area (mm^2)	Published year	Resonance at (GHz)
[21]	$L = 30.08$; $W = 45.9$; $l = 20$; $w = 8$	Two rectangular slots in rectangular patch	1060.672	2012	10.0
[20]	$W = 10$; $L = 13$; $l = 6$; $w = 0.5$; $R_1 = 1.5$; $R_2 = 1$	Rectangular patch with four rectangular slots and one cylindrical slot	111.975	2014	9.1, 10.4
[22]	$W = 18$; $L = 20$; $l = 6$; $w = 2$	Rectangular patch with two rectangular slots	336	2015	9.09, 9.87
[23]	$W = L = 20$; $w = 8$; $l = 4$; $s_1 = 4$; $s_2 = 2$; $h = 3$	Swastika shaped patch	239	2015	9.5
[24]	$W = 49.41$; $L = 41.34$; $l = 6.17625$; $w = 5.1675$	Quad staircase shaped patch	1276.63	2016	9.39
[25]	$L = 30.8$; $W = 20$; $l = 7.3$; $w = 2.56$	Plus shaped slot within rectangular patch	541.48	2016	10.1
[26]	$R = 22.4$	Logo type slot in circular patch	1280 (approx.)	2018	8.78, 10.33
[27]	$L = 14.5$; $W = 15$; $r_1 = 1$; $r_2 = 1.1$; $r_3 = 2.5$; $r_4 = 1.9$	Rectangular patch with four circular cuts at corners	208.025	2018	10.04
[28]	$W = 20.37$; $L = 23.5$; $t = 2.5$	E-shaped patch	358.695	2019	9.18

[29]	$W = 20$; $L = 16$; $l = 31$; $w = 1$	E-shaped slot in rectangular patch	289	2019	8.9, 10.4
[30]	$L = 21.5$; $W = 16.50$	Rectangular patch structure loaded multi-slotted forked antenna	230	2019	10.31
[31]	$L = 29.8$; $W = 39.8$	Modified Hilbert Curve Fractal from rectangular patch	739.38	2020	9.5, 10.0
Fabricated DEMPA	$a_1 = 9.0$; $a_2 = 7.5$; $d = 14.0$	Double elliptical patch	181.335	——	9.0
Where, a — length of semi-major axis of ellipse; b — length of semi-minor axis of ellipse; L — length of rectangle; W — width of rectangle; l — length of slot; w — width of slot; s_1 — length of small slot; s_2 — width of small slot; h — size of square slot; R — radius of circle; t — notch thickness; R_1 — radius of outer circle; R_2 — radius of inner circle; r — radius of circular arc; a_1 — semi-major axis of left half-ellipse of DEMPA; a_2 — semi-major axis of right half-ellipse of DEMPA; d — common minor axis of DEMPA.					

Z axis. The maximum surface current was observed on the feed line and at the lower portion of patch.

The fabricated DEMPA is found to possess less effective patch area than other MSPAs reported in literature for radiolocation applications. This is evident from the comparison table shown above in Table 7 where the resonant frequencies of all the antennas fall within the frequency band of 8.50 GHz–10.55 GHz.

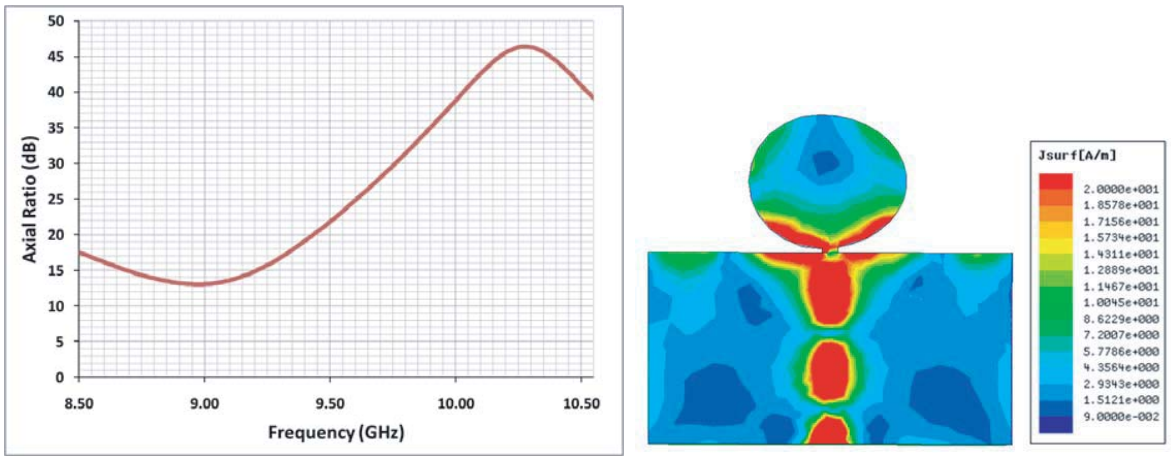

(a) (b)

Figure 9. (a) Simulated Axial Ratio curve, (b) Simulated Surface Current Distribution — for $\text{DEMPA}_{\text{mah}}$ with $a_1 = 9.0\,\text{mm}$, $a_2 = 7.5\,\text{mm}$ and $d = 14.0\,\text{mm}$ within the frequency range for radiolocation applications.

7. CONCLUSION

The statistical technique of Response Surface Methodology (RSM) in Design of Experiments (DOE) was used to study the parametric relationship between the Return Loss (RL) at resonant frequency and the input parameters — length of vertically aligned minor axis (d), the length of semi-major axis of left half-ellipse (a_1), and the length of semi-major axis of right half-ellipse (a_2) — for Double Elliptical Micro-strip Patch Antenna (DEMPA) within the frequency band of 8.50 GHz–10.55 GHz which is earmarked for radiolocation applications. An empirical formula that demonstrates the parametric relationship has been obtained. The predictive ability of regression model was confirmed by using numerical models of two DEMPAs that were not utilized to build the empirical relationship, one among which had been fabricated, tested, and reported in literature. This statistical technique helped to conduct the study with the minimum number of numerical models and simulation runs to draw statistically significant results. The conventional style of varying one input parameter at a time, which needs huge modeling/experimental effort, can be effectively replaced by this statistical method in electromagnetic studies, especially in micro-strip patch antenna design. The important findings are given below.

1. The interdependence between the return loss at resonant frequency and geometric parameters of DEMPA can be described with the help of a statistically significant second order regression model.
2. The RL of $\text{DEMPA}_{\text{mah}}$ increases with the increase in the lengths of its two different semi-major axes. In other words, the more the flatness of DEP_{mah} is over the horizontal direction, the higher its value of return loss will be.
3. With the given patch, feed arrangement, and range of dimensions for a $\text{DEMPA}_{\text{mah}}$, the interaction effects of the input parameters on RL are statistically insignificant.
4. Variation in the length of vertically aligned minor axis (d) within the range selected and with lengths of two semi-major axes kept constant causes the RL to increase till its middle value and then decrease. Thus higher RL values are found to occur at the mean value of d.
5. Antenna miniaturization can be achieved for radiolocation applications by using double elliptical patches.

REFERENCES

1. Donelli, M. and P. Febvre, "An Inexpensive reconfigurable planar array for Wi-Fi applications," *Progress In Electromagnetics Research C*, Vol. 28, 71–81, 2012.
2. Donelli, M., T. Moriyama, and M. Manekiya, "A compact switched-beam planar antenna array for wireless sensors operating at Wi-Fi band," *Progress In Electromagnetics Research C*, Vol. 83, 137–145, 2018.
3. Hansen, R. C., "32-antennas," *Reference Data for Engineers*, 9th Edition, W. M. Middleton and M. E. Van Valkenburg, Eds., 32–1, Woburn, Newnes, 2002.
4. Donelli, M. and F. Robol, "Circularly polarized monopole hook antenna for ISM-band systems," *Microw. Opt. Technol. Lett.*, Vol. 60, No. 6, 1452–1454, 2018, doi: 10.1002/mop.31179.
5. Khan, M. U., M. S. Sharawi, and R. Mittra, "Microstrip patch antenna miniaturisation techniques: A review," *IET Microw. Antennas Amp Propag.*, Vol. 9, No. 9, 913–922, Mar. 2015, doi: 10.1049/iet-map.2014.0602.
6. Jose, J. V., A. Shobha Rekh Paulson, and M. J. Jose, "Double-Elliptical shaped miniaturized microstrip patch antenna for ultra-wide band applications," *Progress In Electromagnetics Research C*, Vol. 97, 95–107, 2019.
7. Jose, J. V., A. Shobha Rekh Paulson, and M. J. Jose, "Double-Elliptical micro-strip patch antenna for higher design flexibility and miniaturization," *Int. J. Eng. Adv. Technol.*, Vol. 9, No. 1, 6970–6976, Oct. 2019.
8. Valentín, E. and R. A. Rodríguez-Solís, "Characterization of a cavity-backed capacitively-fed folded slot antenna using DOE techniques," *2014 IEEE Antennas and Propagation Society International Symposium (APSURSI)*, 1499–1500, Jul. 2014, doi: 10.1109/APS.2014.6905075.

9. Naishadham, K., "Design of experiments as a microwave CAD tool," *Microw. Opt. Technol. Lett.*, Vol. 52, No. 5, 1020–1024, 2010, doi: 10.1002/mop.25133.
10. Saleem, M. M. and A. Somá, "Design of experiments based factorial design and response surface methodology for MEMS optimization," *Microsyst. Technol.*, Vol. 21, No. 1, 263–276, Jan. 2015, doi: 10.1007/s00542-014-2186-8.
11. Akhtar, F., M. M. Saleem, M. Zubair, and M. Ahmad, "Design optimization of RF-MEMS based multiband reconfigurable antenna using response surface methodology," *2018 Progress in Electromagnetics Research Symposium (PIERS-Toyama)*, 743–750, Toyama, 2018, doi: 10.23919/piers.2018.8598186.
12. Chen, Y.-S. and T.-Y. Ku, "Efficiency improvements of antenna optimization using orthogonal fractional experiments," *International Journal of Antennas and Propagation*, Article ID 708163, 2015, https://www.hindawi.com/journals/ijap/2015/708163/, (accessed Mar. 12, 2020).
13. Margaret, D. H. and B. Manimegalai, "Modeling and optimization of EBG structure using response surface methodology for antenna applications," *AEU — Int. J. Electron. Commun.*, Vol. 89, 34–41, May 2018, doi: 10.1016/j.aeue.2018.03.017.
14. Behera, S. K., H. Meena, S. Chakraborty, and B. C. Meikap, "Application of response surface methodology (RSM) for optimization of leaching parameters for ash reduction from low-grade coal," *Int. J. Min. Sci. Technol.*, Vol. 28, No. 4, 621–629, Jul. 2018, doi: 10.1016/j.ijmst.2018.04.014.
15. Bezerra, M. A., R. E. Santelli, E. P. Oliveira, L. S. Villar, and L. A. Escaleira, "Response surface methodology (RSM) as a tool for optimization in analytical chemistry," *Talanta*, Vol. 76, No. 5, 965–977, Sep. 2008, doi: 10.1016/j.talanta.2008.05.019.
16. Vahiddastjerdi, H., A. Rezaeian, M. R. Toroghinejad, G. Dini, and E. Ghassemali, "Optimizing pulsed Nd: YAG laser welding of high-Mn TWIP steel using response surface methodology technique," *Opt. Laser Technol.*, Vol. 120, 105721, Dec. 2019, doi: 10.1016/j.optlastec.2019.105721.
17. Vedrtnam, A., G. Singh, and A. Kumar, "Optimizing submerged arc welding using response surface methodology, regression analysis, and genetic algorithm," *Def. Technol.*, Vol. 14, No. 3, 204–212, Jun. 2018, doi: 10.1016/j.dt.2018.01.008.
18. Peng, L., C. Ruan, and X. Yin, "Analysis of the small slot-loaded elliptical patch antenna with a band-notched for UWB applications," *Microw. Opt. Technol. Lett.*, Vol. 51, No. 4, 973–976, 2009, doi: 10.1002/mop.24247.
19. Montgomery, D. C., *Design and Analysis of Experiments*, 8th Edition, John Wiley and sons, Inc., New York, 2013.
20. Bhadouria, A. S. and M. Kumar, "Microstrip patch antenna for radiolocation using DGS with improved gain and bandwidth," *2014 International Conference on Advances in Engineering Technology Research (ICAETR — 2014)*, 1–5, Aug. 2014, doi: 10.1109/ICAETR.2014.7012873.
21. Aggarwal, K. and A. Garg, "A S-shaped patch antenna for X-band wireless/microwave applications," *International Journal of Computing and Corporate Research*, Vol. 2, No. 2, International Manuscript ID: ISSN2249054X-V2I2M2-032012, 2011.
22. Saini, H., A. Kaur, A. Thakur, R. Kumar, and N. Kumar, "Compact multiband ground slotted patch antenna for X-band applications," *2015 2nd International Conference on Recent Advances in Engineering Computational Sciences (RAECS)*, 1–6, Dec. 2015, doi: 10.1109/RAECS.2015.7453333.
23. Singh, V., B. Mishra, and R. Singh, "A compact and wide band microstrip patch antenna for X-band applications," *2015 Second International Conference on Advances in Computing and Communication Engineering*, 296–300, May 2015, doi: 10.1109/ICACCE.2015.135.
24. Sran, S. S. and J. S. Sivia, "Quad staircase shaped microstrip patch antenna for S, C and X band applications," *Procedia Comput. Sci.*, Vol. 85, 443–450, Jan. 2016, doi: 10.1016/j.procs.2016.05.190.
25. Jayasree, S. J. and S. Saravanan, "Miniaturized slotted patch antenna for X-band apllications," *Int. J. Eng. Res. Technol.*, Vol. 4, No. 14, Jul. 2018, [Online]. Available: https://www.ijert.org/research/miniaturized-slotted-patch-antenna-for-x-band-apllications-IJERTCONV4IS14010.pdf, https://www.ijert.org/miniaturized-slotted-patch-antenna-for-x-band-apllications, (accessed: Jul. 10, 2020).

26. Kaushal, D. and T. Shanmuganantham, "Design of a compact and novel microstrip patch antenna for multiband satellite applications," *Mater. Today Proc.*, Vol. 5, No. 10, Part 1, 21175–21182, Jan. 2018, doi: 10.1016/j.matpr.2018.06.516.
27. Sharma, I. B., F. L. Lohar, R. K. Maddila, A. Deshpande, and M. M. Sharma, "Tri-band microstrip patch antenna for C, X, and Ku band applications," *Optical and Wireless Technologies*, 567–574, Singapore, 2018, doi: 10.1007/978-981-10-7395-3_63.
28. Sharma, S. K. and Y. Kumar, "E-shaped micro-strip notched patch antenna for wireless applications," Art. No. 1696, Oct. 2019, [Online]. Available: https://easychair.org/publications/preprint/rhNZ, (accessed: Jul. 20, 2020).
29. Khan, I., G. D. Devanagavi, S. K. R, R. R. K, R. Gunjal, and T. Ali, "A hepta-band antenna loaded with E-shaped slot for S/C/X-band applications," *Int. J. Electron. Telecommun.*, Vol. 65, No. 2, Art. No. 2, May 2019.
30. Godaymi, W. A., R. M. Shaaban, Al-Tumah, A. S. Tahir, and Z. A. Ahmed, "Multi-forked microstrip patch antenna for broadband application," *J. Phys. Conf. Ser.*, Vol. 1294, 022020, Sep. 2019, doi: 10.1088/1742-6596/1294/2/022020.
31. Kumar, A. and A. P. S. Pharwaha, "Development of a modified Hilbert curve fractal antenna for multiband applications," *IETE J. Res.*, Vol. 0, No. 0, 1–10, Jun. 2020, doi: 10.1080/03772063.2020.1772126.